Mechanism of $[M + H]^+$ Formation in Photoionization Mass Spectrometry

Jack A. Syage
Syagen Technology, Inc., Tustin, California, USA

In this paper we examine the mechanism of $[M + H]^+$ (henceforth MH^+) formation by direct photoionization. Based on comparisons of the relative abundance of M^+ and MH^+ ions for photoionization of a variety of compounds M as vapor in air versus in different solvents, we conclude that the mechanism is $M + h\nu \rightarrow M^+ + e^-$ followed by the reaction $M^+ + S \rightarrow MH^+ + S(-H)$. The principal evidence for molecular radical ion formation M^+ followed by hydrogen atom abstraction from protic solvent S are: (1) Nearly exclusive formation of M^+ for headspace ionization of M in air, (2) significant relative abundance of MH^+ in the presence of protic solvents (e.g., CH_3OH, H_2O, c-hexane), but not in aprotic solvents (e.g., CCl_4-), (3) observation of induced equilibrium oscillations in the abundance of MH^+ and M^+, and (4) correlation of the ratio of MH^+/M^+ to reaction length in the photoionization source. Thermodynamic models are advanced that explain the qualitative dependence of the MH^+/M^+ equilibrium ratio on the properties of solvent S and analyte M. Though the hydrogen abstraction reaction is endothermic in most cases, it is shown that the equilibrium constant is still expected to be much greater than unity in most of the cases studied due to the very slow reverse reaction involving the very low abundant MH^+ and S(−H) species. (J Am Soc Mass Spectrom 2004, 15, 1521–1533) © 2004 American Society for Mass Spectrometry

The use of photoionization (PI) in analytical mass spectrometry is a relatively new development [1]. The introduction of compact, sensitive PI sources for commercial analytical MS instruments at atmospheric pressure (e.g., atmospheric pressure photoionization, APPI) [2, 3, 4] and sub-atmospheric pressure (e.g., low pressure photoionization, LPPI) [5, 6, 7] have opened up new applications and areas of research. APPI is by far the most widely utilized embodiment owing to the widespread use of LC/MS (for recent review articles see [8, 9]). APPI is a valuable complement to atmospheric pressure chemical ionization (APCI) and electrospray ionization (ESI) and is helping to extend the range of molecules that can be efficiently ionized. However, it is fair to say that the growth in usage of APPI and development of new applications is outpacing work to understand the fundamental mechanism of PI at elevated pressures [10, 11, 12].

The basic mechanism of photoionization is $M + h\nu \rightarrow M^+ + e^-$. However, the predominant ion observed by APPI is typically $[M + H]^+$ (henceforth MH^+). This would indicate the involvement of a chemical reaction following the photoionization event. In some instances, which seem to correlate with molecules of low proton affinity, the molecular ion M^+ is observed. It is known from studies of photoionization under collisionless conditions in vacuum that M^+ is typically formed [13]. However, it is not certain whether this process dominates at atmospheric pressure. There are two general mechanisms possible for production of MH^+ from M.

$$M + R^+ \rightarrow MH^+ + R(-H) \quad \text{(protonation by charge carrier } R^+\text{)} \tag{1}$$

$$M^+ + S \rightarrow MH^+ + S(-H) \quad \text{(hydrogen atom abstraction from a protic molecule S)} \tag{2}$$

The protonation mechanism is the basis for APCI and ESI. The protonation mechanism is also believed to dominate for dopant APPI where the charge carrier is formed by photoionization of an abundant species R (e.g., toluene and acetone), which then ionizes analyte M [2, 14]. For direct APPI (e.g., in the absence of dopant), the available data is not sufficient to ascertain which of these mechanisms dominates or whether the two mechanisms can occur in parallel. However, there is a tendency in the literature to ascribe the protonation mechanism to dopant and direct APPI alike [15].

In order to understand the APPI mechanism of MH^+ formation and draw a correspondence to the fundamental

Published online September 18, 2004
Address reprint requests to Dr. J. A. Syage, Syagen Technology, Inc., 1411 Warner Avenue, Tustin, CA 92780, USA. E-mail: jsyage@syagen.com

1044-0305/04/$30.00
doi:10.1016/j.jasms.2004.07.006

Received April 30, 2004
Revised July 7, 2004
Accepted July 8, 2004

PI process in vacuum, we have performed a series of experiments using a low-pressure PI (LPPI) source. We have chosen several unsubstituted polyatomic hydrocarbons for their low-polarity and included some compounds with polar substituent groups in order probe the MH^+/M^+ ratio as a function of polarity and proton affinity. In the Results section we present a comparison of the PI MS of these compounds under headspace vapor sampling and by liquid vaporization sampling with a variety of solvents. In the Discussion section, we investigate the thermochemical properties of ionization and subsequent reactions. These results provide strong evidence that the dominant mechanism of MH^+ formation by PI is that of hydrogen abstraction by M^+ in a collisional environment containing protic solvent molecules [i.e., reaction (eq 2)].

Experimental

The experimental results were recorded on a Syagen Radiance Pro low-pressure photoionization (LPPI), quadrupole ion trap, time-of-flight (QitTof) mass spectrometer (MS) system. The LPPI source operates at about 1–4 torr. The details of the MS are less relevant to this work than that of the LPPI source, but some information is warranted. Ions exit the LPPI source and are focused into the ion trap where they are stored at about 1 mtorr under a buffer gas that is either air headspace air sampling or solvent from liquid injection. The trapped ions are then injected into a reflectron TOFMS by turning off the trap RF and applying positive and negative high voltage pulses to the entrance and exit endcaps of the ion trap. The store and eject period is operated at 60 Hz. The duration of the eject cycle is determined by the RF shutoff time of about 100 μs; hence the duty cycle for collection and storage of ions is greater than 99%. The reflectron TOFMS has a total drift length of about 1.2 m and was operated in this work at a resolution of 1000–1500 (m/Δm FWHM). The PI MS spectra reported here were generally collected for 10 s, which at 60 Hz corresponds to 600 accumulated spectral acquisitions.

Continuous infusion was used for both gaseous headspace sampling and liquid sampling. For headspace sampling, a 3 in. long, 100 μm i.d. stainless tube was used to deliver an air flow rate of 5 cm^3 atm/min. For liquid sampling a 3 ft. long, 62 μm ID PEEK tube was used to deliver a liquid flow rate of 8–10 μL/min. On a molar basis the air and liquid flow rates were within a factor of two of each other. The PEEK tubing was connected to a stainless needle through a zero volume union. The stainless needles of these continuous flow samplers penetrate a septum interface to deliver the sample to the LPPI ionization region. Some measurements (as noted later) were made using syringe injection through the septum interface. The temperature of the LPPI source was set at 220 °C. Vapor sample was prepared by adding 10–50 mg of compound to a 4 mL vial with a septum cap. The stainless steel sampling tube was inserted through the septum cap along with another vent tube to maintain constant pressure in the sample vial. The vial and sampling tube were then heated until a clearly detectable signal was observed. Based on prior knowledge of signal intensity for calibrated samples, we estimate that the different heating rates applied to each sample generated headspace vapor pressures on the order of 10 ppm in air.

The PI light source is an RF discharge lamp that is essentially identical to commercial APPI sources (Syagen PhotoMate) used for LC/MS instruments. We provide additional details on the LPPI source because the ionization and drift volumes in the source impact results presented later. Photoions are focused onto a skimmer-like exit electrode. A total of three cylindrical electrodes define two regions. The region closer to the PI lamp is where a large majority of the detected ions are formed. The region closer to the exit electrode is a drift region where the ions are focused to optimize their transmission efficiency through the skimmer cone. The total internal volume of the LPPI source is about 1 cm^3. At a pressure of 2 torr, the ions of MW in the 100–200 range undergo about 4000 collisions with the background gas before exiting the LPPI source. The residence time of the ions in the source is less than 1 ms based on an ion-mobility calculation; [$v = K \times E$ where the ion mobility for a typical ion of mass m/z 200 is $K \approx 1\ cm^2/V{\cdot}s$ at 1 atm and is proportional to gas density (at least when $kT >>$ imparted ion energy, which is not rigorously true here), such that at 2 torr $K \approx 0.003\ cm^2/V{\cdot}s$. E in the LPPI source is about 15 V/cm. This gives $v \approx 5700$ cm/s and for a source length of 1 cm gives a drift time of about 0.18 ms] [16].

Table 1 lists the compounds used in this work and the media (e.g., air or solvent) and concentrations in which they were introduced into the LPPI/MS system.

Results

Headspace Vapor Versus Solvent Liquid Measurements

Headspace vapor samples were recorded in order to observe the ion mass spectra of the test compounds in the absence of solvent. These spectra, of which the parent ion region is shown in Figure 1, are characterized by the presence of a predominant molecular radical ion M^+ and the near absence of fragment ions. As noted previously, the headspace concentration for these measurements was on the order of 10 ppm. To test whether the mass spectra depended on vapor concentration, we varied the heating rate for some of the compounds to give signal intensity spanning about two orders of magnitude and observed no significant changes in the ion distributions.

The mass spectra of the test compounds in MeOH were also recorded to assess the changes in M^+ and MH^+ ion distributions due to the presence of a protic solvent. The results in the absence and presence of

Table 1. Tabulation of compounds and conditions

Compound	MW	Sample	Concentration range	$MH^+/[M^+ + MH^+]$ ratio[a]
Naphthalene	128	Headspace, MeOH	0.1–1000 μg/mL	0
1-Aminonaphthalene	143	Headspace, MeOH, EtOH, i-PrOH, H_2O, c-hexane, CH_2Cl_2, C_2HCl_3, CCl_4	0.1–1000 μg/mL	0.80
2-Aminobiphenyl	169	Headspace, MeOH	10–1000 μg/mL	0.95
Anthracene	178	Headspace, MeOH	10–1000 μg/mL	0.85
Phenanthrene	178	Headspace, MeOH, EtOH, i-PrOH, c-hexane, CH_2Cl_2, C_2HCl_3	1–1000 μg/mL	0.35
Pyrene	202	Headspace, MeOH	10–1000 μg/mL	0.90
Fluoranthene	202	Headspace, MeOH	10–1000 μg/mL	0.60
Benzo[a]pyrene	252	Headspace, MeOH	10–1000 μg/mL	0.95

[a]Ratio in the presence of compound in MeOH at 1000 μg/mL. Qualitative values rounded to nearest 0.05.

MeOH (i.e., headspace sample and vaporized liquid sample, respectively) are plotted in Figure 1. Table 1 summarizes the MH^+ yield for the compounds in MeOH. The naphthalene PI mass spectrum is essentially unchanged in the presence or absence of MeOH and gives a predominant M^+ ion. Intermediate cases showing a significant presence of both M^+ and MH^+ include phenanthrene and fluoranthene. The strong case where a predominance of MH^+ is observed includes 1-aminonaphthalene, 1-aminobiphenyl, anthracene, pyrene, and benzo[a]pyrene.

The linearity of the M^+ and MH^+ with concentration of 1-aminonaphthalene in methanol was measured by syringe injection and capillary infusion. Figure 2a shows a linear response over the 3-decade range of concentration range 0.1 to 100 μg/mL. The ratio of MH^+/M^+ is plotted in Figure 2b and shows that the value is relatively constant by either syringe injection or capillary infusion. These results indicate that the MH^+/M^+ equilibrium is not significantly affected by the analyte concentration and therefore not dependent on self-reaction over this concentration range. (The

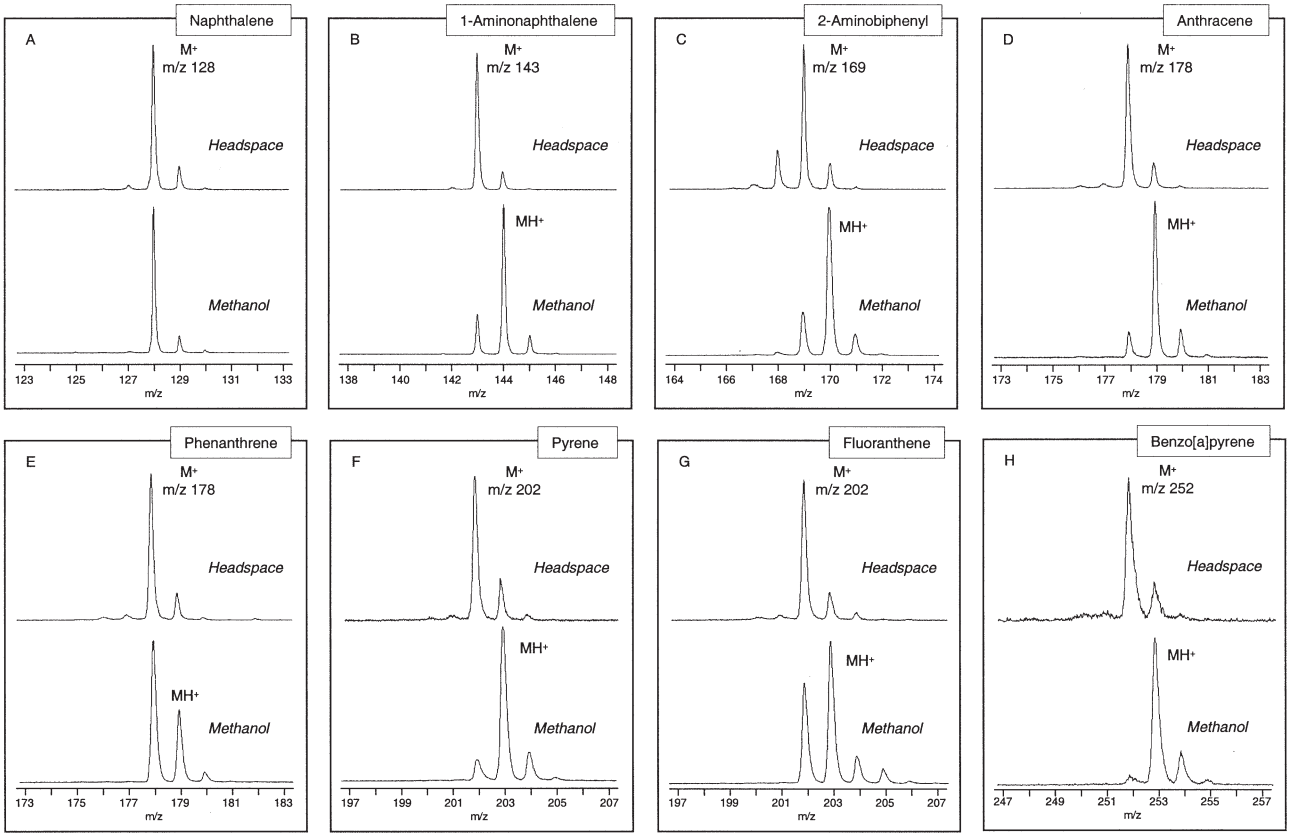

Figure 1. Comparison of PI MS spectra in the parent ion region for analyte as headspace in air versus in the presence of vaporized MeOH solvent. These spectra show the difference in photoionization distribution due to the presence of MeOH.

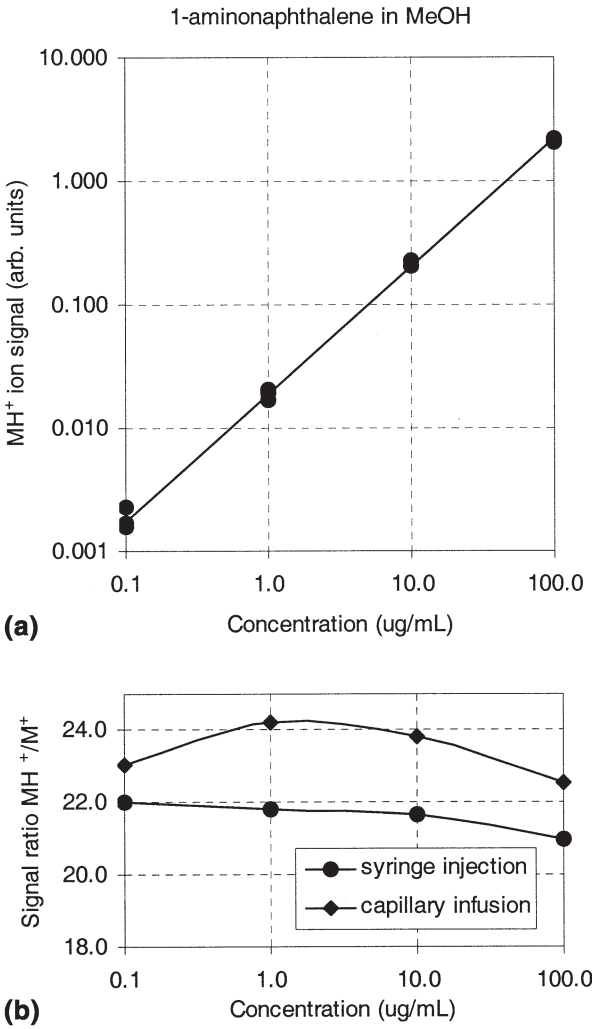

Figure 2. (**a**) Linearity plot of the predominant MH^+ ion intensity for PI of 1-aminonaphthalene in MeOH. Plotted points represent triplicate measurements. (**b**) Measured ion signal ratio MH^+/M^+ as a function of concentration for two different methods of sample introduction.

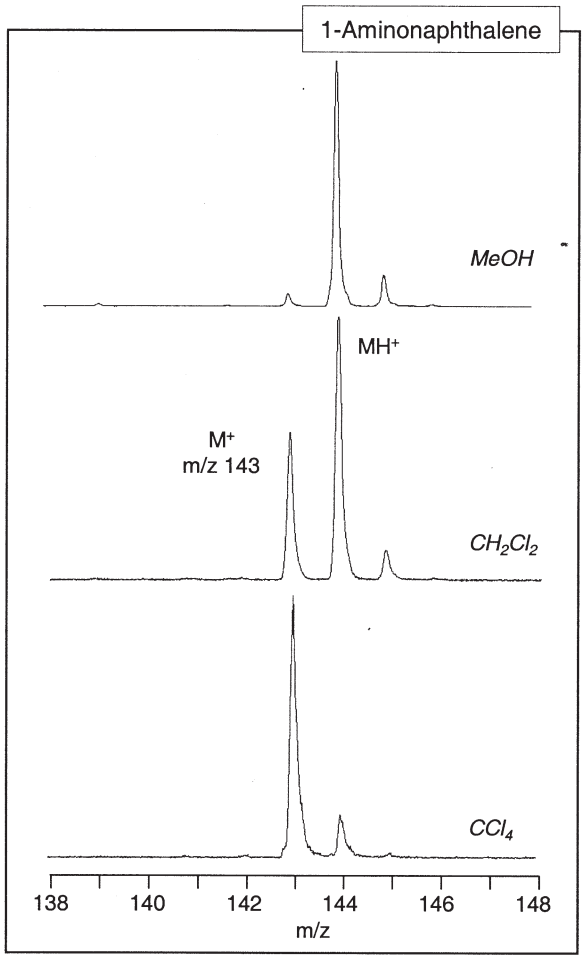

Figure 3. Examples of PI MS spectra for 1-aminonaphthalene in different solvents showing the dependence of the M^+ and MH^+ distribution with solvent.

dependence of MH^+/M^+ on analyte concentration is considered further in a later section.)

Dependence on Solvent

The dependence of the MH^+/M^+ ratio was measured for different solvents. We focused on 1-aminonaphthalene and phenanthrene since these compounds had relative MH^+ abundances that were not at the extreme end of the scale of 0 to 1 (see Table 1). Additional measurements were conducted for the compounds naphthalene, aniline, phenol, toluene, and benzoic acid in MeOH, H_2O, c-hexane, and CCl_4 and are reported in the Discussion in the context of predicted thermochemical properties.

Mass spectra for 1-aminonaphthalene in different solvents are shown in Figure 3 and the results of the MH^+/M^+ measurements for 1-aminonaphthalene and phenanthrene are presented in Figure 4. There is a clear trend toward increased MH^+/M^+ ratio for protic solvents. Some caution must be taken with this data because the M^+ versus MH^+ ions may react with solvent to form other ion products and these reactions may skew the relative M^+ and MH^+ distribution. Ion molecule reactions were evident in the solvents, i-PrOH, CH_2Cl_2, C_2HCl_3 (trichloroethylene), and to a lesser extent CCl_4. The absolute total ion signal (M^+, MH^+, and other evident M derived ion products) was within a factor of two for the different solvents. This suggests that the ionization efficiency is primarily a function of the concentration of M, and the photon flux. The parent ion is presumed to be M^+.

Varying MH^+/M^+ Equilibrium

Induced vapor pressure oscillations. The capillary infusion inlet consists of a liquid stream that exits a capillary into the low pressure PI source. The liquid stream is typically not smooth due to the tendency of droplets to form at the capillary exit. Based on real-time profiling of ion signals, it is believed that these droplets break off

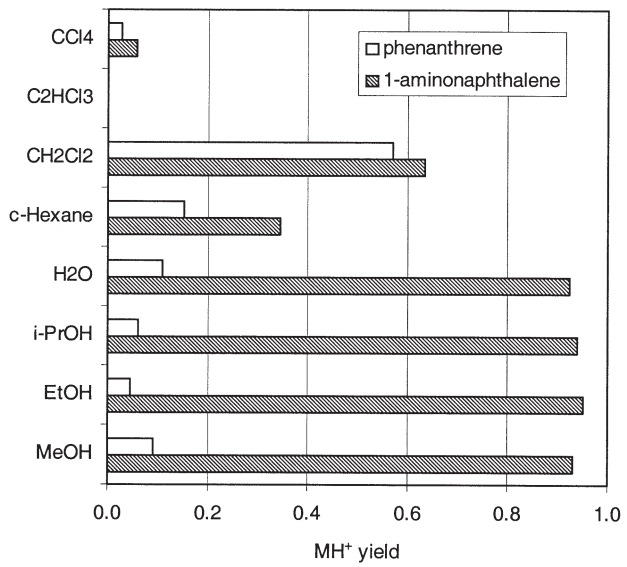

Figure 4. Bar plot of the MH^+ yield = $[MH^+]/([M^+] + [MH^+])$ for phenanthrene and 1-aminonaphthalene in various solvents. The phenanthrene in H_2O sample did not give stable signal possibly due to solubility problems. The measured MH^+ yields for 1-aminonaphthalene and phenanthrene in C_2HCl_3 were slightly negative after correcting for the ^{13}C distribution, which is zero within experimental error.

from the exit in a more or less repetitive manner where they then flash vaporize on the heated LPPI surfaces. Under certain conditions this effect can be quite oscillatory. The oscillating behavior of the liquid vapor pressure provides a convenient means to investigate the dependence of the MH^+/M^+ equilibrium ratio on solvent vapor density in the LPPI source.

Figure 5 shows the M^+, MH^+, and sum signal for 1-aminonaphthalene in c-hexane as a function of the oscillating solvent vapor pressure in the LPPI source. The most significant observation is the oppositely-phased oscillations of the M^+ and MH^+ signal and the nearly constant sum signal. Furthermore the MH^+ signal peaks at what are believed to be pressure peaks in the vaporized liquid stream. This conclusion is reached because the peaks have the appearance of a droplet vaporization followed by a decay that is exponential in shape with a decay time matching the estimated residence time of vapor in the LPPI source. [It should be noted that these oscillations are not always exponential in appearance]. Similar oppositely-phased oscillations of the M^+ and MH^+ signal were also observed for phenanthrene. It is further interesting to note that for phenanthrene, ion signal at *m/z* 83 and 84, respectively, match the dependence of M^+ and MH^+ suggesting that these fragment ions are derived from the respective parent ions.

The results in Figure 5 for 1-aminonaphthalene and corroborated for phenanthrene are compelling evidence that MH^+ derives from M^+ and is not formed by an independent ionization mechanism from M. Because this derivation is a function of solvent vapor concentration, we infer that the transformation of M^+ to MH^+ is due to H atom abstraction from the solvent c-hexane.

LPPI flow-tube reactor. We further investigated the kinetics of the presumed mechanism of reaction (eq 2)

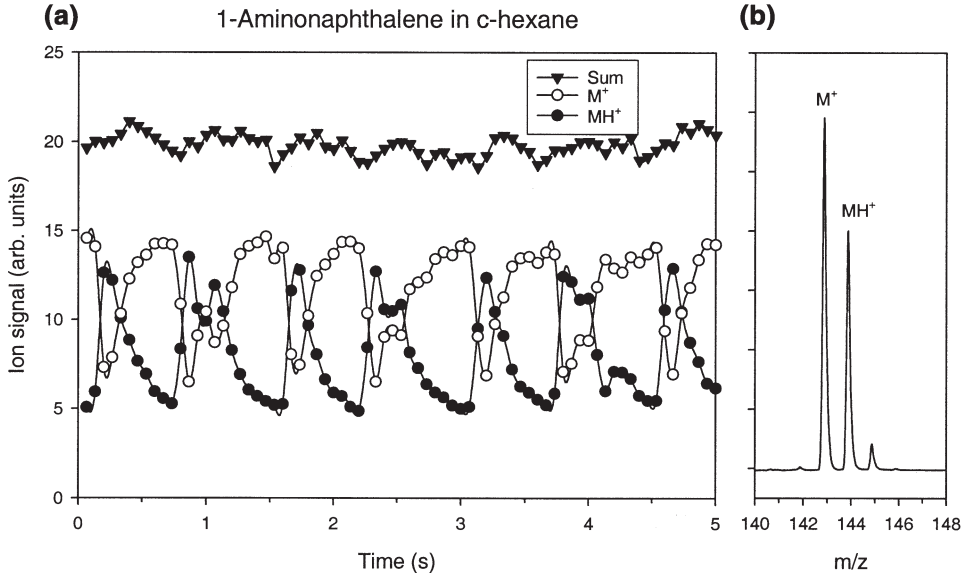

Figure 5. Example of the effect of induced fluctuations of the MH^+/M^+ equilibrium distribution generated by the pulsating liquid stream injection of the capillary infusion line for 1-aminonaphthalene in c-hexane. (**a**) Selected ion monitoring (SIM) of M^+, MH^+, and the sum intensity. The relatively constant sum intensity $MH^+ + M^+$ is strong evidence for a process of $M^+ \rightarrow MH^+$ and not an independent mechanism to forming MH^+. (**b**) The accumulated PI MS spectrum.

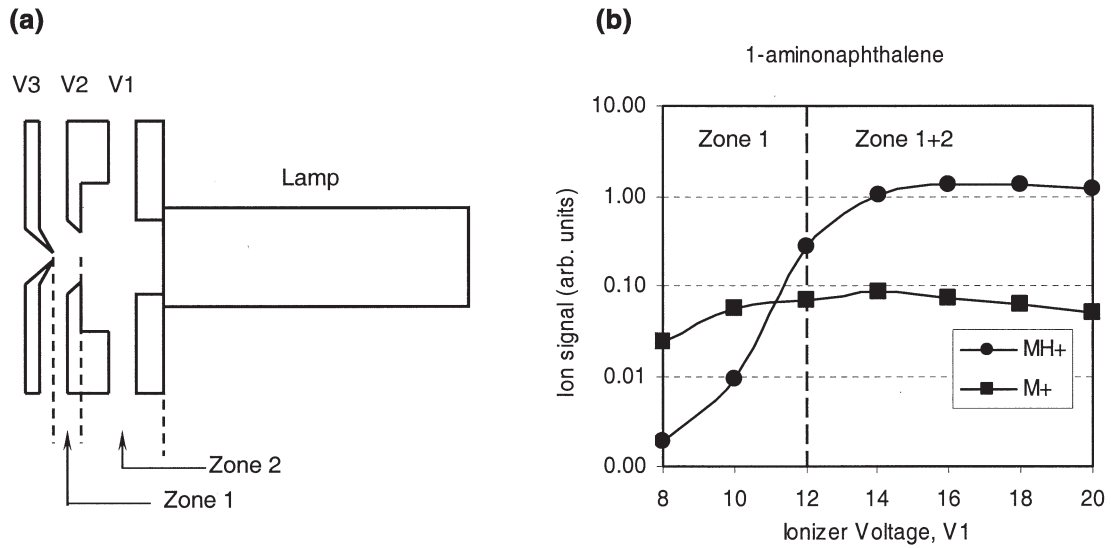

Figure 6. Measurements of the M^+ and MH^+ signal for PI of 1-aminonaphthalene in MeOH from different regions of the LPPI source. (**a**) Cross section of the LPPI source showing Zone 1 and Zone 2 where initially-formed M^+ ions experience different reaction lengths before exiting the V3 aperture. (**b**) M^+ and MH^+ intensities in Zones 1 and 2 showing less conversion to MH^+ in Zone 1 where the reactive length is short relative to Zone 2. Intensity axis is on a log scale.

by operating the LPPI source as a low pressure flow-tube reactor. As seen in Figure 6a the three electrodes in the LPPI source define two regions or zones at different distances from the exit aperture. If the operative mechanism is H atom abstraction [reaction (eq 2)] then one should expect the MH^+/M^+ ratio to be a function of the reactive length that the ions have traveled. Upon exiting the LPPI source, the pressure is sufficiently low that no further reactions occur.

It is possible to probe the relative MH^+ and M^+ distributions by varying the V1 voltage so as to vary the efficiency of detecting ions from the far zone (i.e., Zone 2). The standard operating voltages on the LPPI source are V1 = 20 V, V2 = 13 V, and V3 = 3 V. These voltages provide optimal ion transmission efficiency for the near and far zones (Zones 1 and 2, respectively) through the exit aperture. For values of V1 > V2, ions are detected from both Zones 1 and 2. For values of V1 < V2, ions in Zone 2 are impeded from exiting the LPPI source; hence the detected ions are predominantly from Zone 1, where the reactive length is minimal.

Figure 6b shows the results for the M^+ and MH^+ signals for a 10 μg/mL sample of 1-aminonaphthalene in MeOH as a function of the LPPI V1 voltage. For V1 voltages where the detected ions originate only from Zone 1, M^+ gives the dominant signal. On the other hand, for V1 voltages where Zone 2 ions are also detected, MH^+ gives the dominant signal. These results provide strong evidence that H atom abstraction by M^+ [reaction (eq 2)] is the predominant mechanism for MH^+ formation. It is interesting to note that if the assumption above that the ions in the LPPI source typically undergo a few thousand collisions, then the ions formed in Zone 1 that give predominantly M^+ undergo at least a few hundred collisions with solvent molecules. This indicates that the reaction probability is rather low.

Kinetic Effects

To further substantiate that reaction (eq 2) occurs in the LPPI source (and therefore under higher pressure conditions such as an APPI source), we have made measurements to rule out the formation of MH^+ in other potentially reactive regions such as the ion trap. Kinetic effects in the ion trap can be explored by varying the ion accumulation time, in effect varying the time that injected ions have to react before they are mass analyzed in the TOFMS. All measurements reported in this paper were recorded at 60 Hz, corresponding to a cycle time in the ion trap of 16.7 ms. Typically, ions are accumulated for the first 15 ms of this interval. Mass analysis is achieved by turning off the ion trap RF amplitude for 0.1–0.2 ms at the end of the interval during which time a 2–4 μs pulsed extraction field is activated to inject the ions into the TOFMS. The accumulated ions therefore reside in the ion trap for 1.5 to 16.5 ms.

To examine whether the MH^+ and M^+ ion abundances are affected by their residence time in the ion trap we measured the ion abundances as a function of accumulation time. Figure 7 shows the results for a sample of 10 μg/mL samples of 1-aminonaphthalene in CCl_4 and MeOH, representing the cases for minimal and maximal formation of MH^+. As expected the signal strength is linearly dependent on the accumulation time. More importantly, the measured value of the MH^+/M^+ ratio for both solvents in Figure 7 is constant

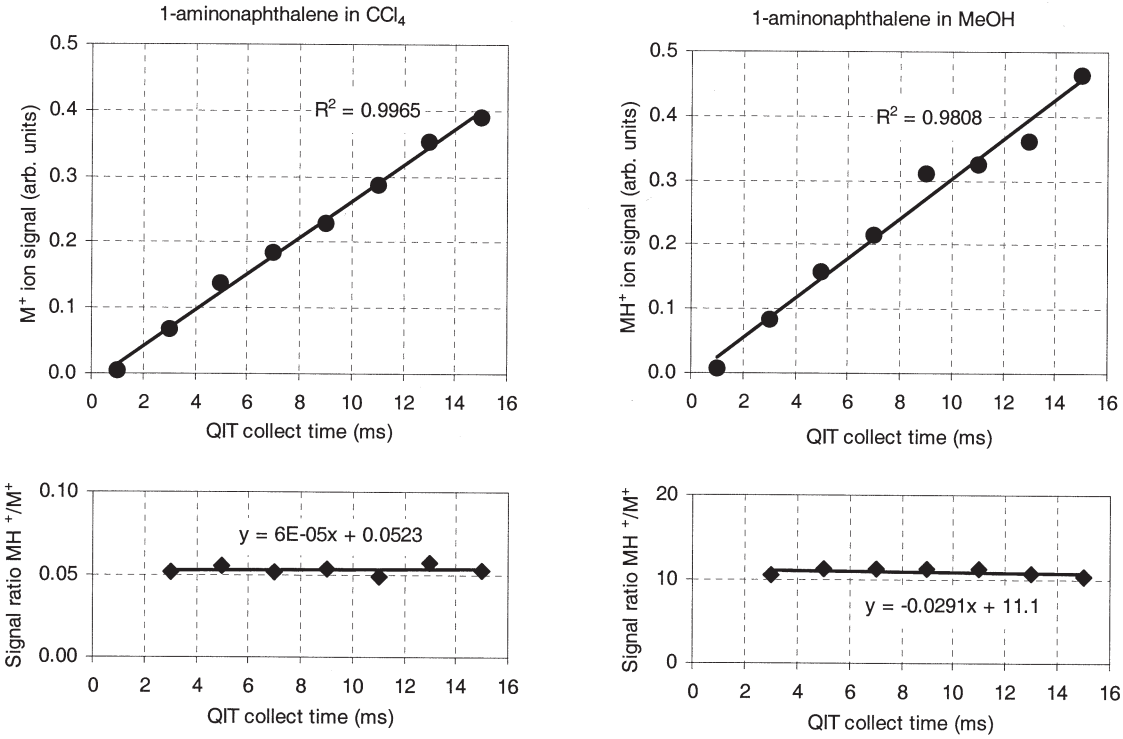

Figure 7. Ion signal intensity as a function of QIT collection time for PI of 1-aminonaphthalene. (Top) Intensity of the predominant ion M^+ for CCl_4 and MH^+ for MeOH. The intensities are linear with collection time as expected. (Bottom) Signal ratio MH^+/M^+ showing constant value indicating minimal change in equilibrium distribution in the QIT.

with accumulation time indicating that no significant interconversion or reaction is occurring in the ion trap.

Discussion

Thermochemical Model

We begin with a simple thermochemical model for estimating the enthalpy ΔH of the dissociative hydrogen transfer (DHT) reaction

$$M^+ + S \rightarrow MH^+ + S(-H) \quad \Delta H \tag{3}$$

This reaction may be expressed by the thermochemical cycle

$$M^+ + e^- \rightarrow M \quad -IE(M) \tag{4a}$$

$$S \rightarrow S(-H) + H \quad D_H(S) \tag{4b}$$

$$H \rightarrow H^+ + e^- \quad IE(H) \tag{4c}$$

$$M + H^+ \rightarrow MH^+ \quad -PA(M) \tag{4d}$$

Where IE is the ionization potential energy, D_H is the H-atom bond (dissociation) energy, and PA is the proton affinity. The enthalpy of the DHT reaction (eq 3) can then be expressed as

$$\Delta H = IE(H) - IE(M) - PA(M) + D_H(S) \tag{5}$$

Table 2 summarizes the thermochemical data that could be found for the test compounds (we could not find adequate data for 1-amino biphenyl and benzopyrene) [17]. Interestingly, compounds with increased proton affinity relative to similar compounds (e.g., 1-aminonaphthalene versus naphthalene; anthracene versus phenanthrene, pyrene versus fluoranthene) also tend to have lower IE value, which has the effect of negating the proton affinity dependence on ΔH. [The qualitative explanation is that properties of a molecule that can stabilize a positive charge, such as a proton, will also stabilize the formation of a positive charge, namely the loss of an electron by M to form a molecular ion M^+. Therefore, PA(M) will tend to be anti-correlated with IE(M)]. Figure 8 shows the correlation of the observed ratio $[MH^+]/([M^+]+[MH^+])$ = MH^+ yield to PA(M) and IE(M). It is clear that MH^+ yield correlates well to PA(M), but not to IE(M) even though both are of equal importance in calculating ΔH by eq 5. In fact the MH^+ yield appears anti-correlated to IE [due to the anti-correlation of PA(M) and IE(M)]. This may indicate that proton affinity may have a stronger effect on the kinetics of the reaction than ionization potential, though this is conjecture at this time.

Because there was insufficient thermochemical data for all the test compounds in Table 1, and in order to

Table 2. Table of thermochemical data used for the model calculations (units are eV)[a]

Molecule	PA	IE	D_H
Phenol	8.51	8.47	
Aniline	9.09	7.72	
Toluene	8.23	8.82	
Benzoic acid	8.59	9.47	
Naphthalene	8.44	8.14	
1-aminonaphthalene	9.41	7.1	
Phenanthrene	8.56	7.89	
Anthracene	8.98	7.45	
Fluoranthene	8.59	7.9	
Pyrene	9.01	7.41	
Benzo[a]pyrene		7.12	
CH_3OH[b]	7.89	10.84	4.08
EtOH[b]	8.17	10.48	4.03
i-PrOH[b]	8.29	10.12	3.95
H_2O	7.36	12.62	5.16
c-C_6H_{12}			4.29
CH_2Cl_2			4.29
$CHCl_3$			4.15
H		13.6	

[a]Values are from Lias, S. G.; Liebman, J. F.; Levin, R. D. J. Phys. Chem. Ref. Data **1984,** *13,* 695 [proton affinity data]; Lias, S. G.; Bartmess, J. E.; Liebman, J. F.; Homes, J. L., Levin, R. D.; Mal-lard, W. G. J: Phys. Chem. Ref. Data 1988, 17, 1 [ionization potential and proton affinity data]; McMillen, D. F.; Golden, D. M. Ann. Rev. Phys. Chem. **1982,** *33,* 493 [bond energy data]. Also NIST Chemistry WebBook, NIST Standard Reference Database Number 69, March 2003 Release. [1 eV/molecule = 23.06 kcal/mol].
[b]Lower H bond energy is for C–H bonds. The O–H bond energy is 4.52 eV.

explore this model for a wider range of substituent groups, we chose a representative set of molecules consisting of naphthalene, aniline, phenol, toluene, and benzoic acid. The pertinent thermochemical data is also presented in Table 2. Using this data we have calculated ΔH for the DHT reaction (eq 3) as a function of $D_H(S)$ in order to obtain a qualitative understanding of the dependence of the MH^+/M^+ ratio as a function of analyte molecule M and solvent S. The calculated energies and dependences are plotted in Figure 9 and predict for the range of molecules that naphthalene ion is least likely and benzoic acid ion most likely to undergo DHT with solvent S to form MH^+. The thermochemical properties of M that favor DHT reaction (eq 3) are large values of IE(M) and PA(M) and the property of S that favors DHT is a small value of $D_H(S)$.

The qualitative predictions of Figure 9 were tested for the five compounds in the solvents MeOH, H_2O, c-hexane, and CCl_4. The latter aprotic solvent was chosen to confirm that M^+ is formed with similar efficiency as the summed intensity $M^+ + MH^+$ in protic solvents, an observation that was true for the compounds reported earlier in Table 1. The experimental data are summarized in Table 3. As noted earlier, certain solvents can further react with the M^+ and MH^+ analyte ions, which can distort the MH^+/M^+ ratio. We therefore report only ratios [expressed as $MH^+/(MH^+ + M^+)$] where clean and distinct spectra were recorded.

The results in Table 3 are consistent with the calculated energetics of DHT reaction as a function of analyte

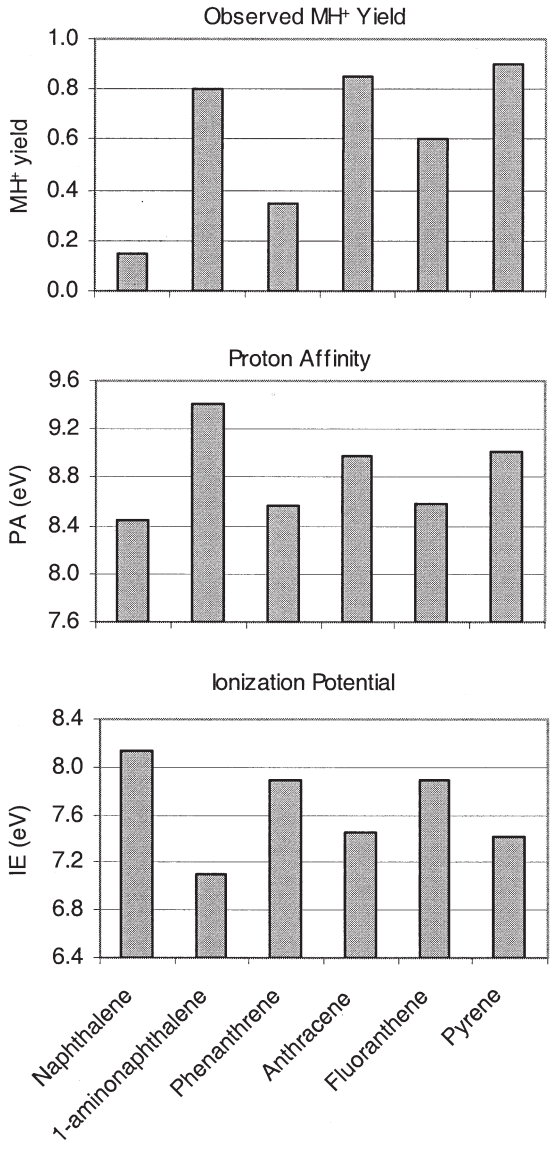

Figure 8. Correlation of the observed MH^+ yield = $[MH^+]/([M^+] + [MH^+])$ for photoionization of M in MeOH to proton affinity and ionization potential.

molecule. Naphthalene indeed shows the lowest yield of MH^+ and benzoic acid the greatest yield. The other analyte molecules follow the trend with the notable exception of aniline, which yields a greater abundance of MH^+ than the simple model would predict. The dependence on solvent is also consistent with the DHT model with the exception of H_2O, which is predicted to be a poor H-atom donor because of its high dissociation energy D_H. There are two other physical properties not considered in our simple bimolecular reaction model that might increase the efficiency of H_2O for the DHT reaction: (1) H_2O is expected to form a strong ion-molecule complex with basic ions (e.g., M^+S complex), and (2) H_2O forms a strong hydrogen bonding network, particularly when bound to an ion, which could facilitate H-atom transfer. These ion-molecule complexation mechanisms are discussed below.

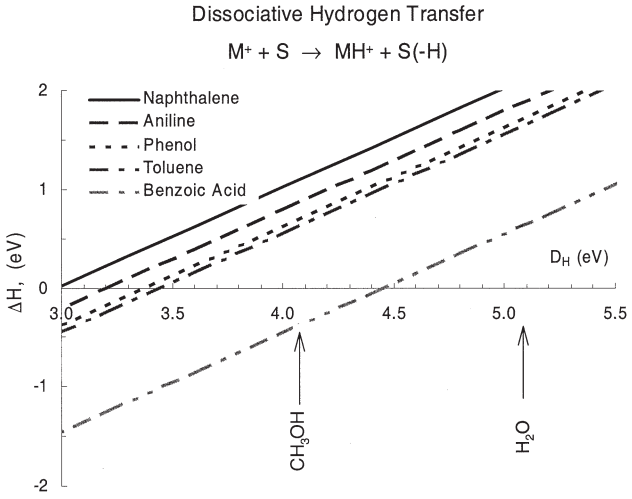

Figure 9. Thermochemical model for Dissociative Hydrogen Transfer (DHT) of various analyte ions as a function of solvent H atom bond energy.

Equilibrium Model

Despite the good qualitative agreement of the experimental results with the predictions of the simple DHT thermochemical model, it should be noted that except for the benzoic acid ion, the DHT reaction is calculated to be endothermic for all the solvents studied. Based on energetics alone, it would appear that the DHT reaction is unfavorable in most cases. However, it becomes clearer why the DHT reaction (eq 3) proceeds when we consider the equilibrium properties.

We start with the standard expression for equilibrium;

$$K = \frac{[MH^+][S(-H)]}{[M^+][S]} = e^{-\Delta G/kT} = e^{-(T\Delta S + \Delta H)/T} \approx e^{-\Delta H/kT} \tag{6}$$

Table 3. Observed MH^+ yield for the test analytes in different solvents

	MeOH	H_2O	c-hexane	CCl_4
Naphthalene	0.15	[a]	0.04	0.06
Aniline	0.98	0.89	0.14	0.11
Phenol	0.01	0.11	0.04	[b]
Toluene	[c]	0.97	[d]	0.10[e]
Benzoic acid	[f]	0.99	0.99	[g]

[a]No significant signal observed.
[b]No signal observed for 10 and 1000 ug/mL; other significant ions observed are CCl_3^+ (m/z 117, 119, 121, 123) and PhO-CCl_2^+ (m/z 175, 177, 179).
[c]No signal observed for 10 ug/mL; strong signal observed for 1000 ug/mL at m/z 91, 92, 93 in approximate proportion of 1.0:0.6:0.1.
[d]Strong signal observed for 10 ug/mL and 1000 ug/mL at m/z 91, 92, 93 in approximate proportion of 1.0:0.7:0.3.
[f]No signal observed for 10 ug/mL; signal observed for 1000 ug/mL; other significant ions observed are m/z 105, 137, 155
[e]No signal observed for 10 ug/mL; signal observed for 1000 ug/mL; other significant ions observed are m/z 91, and toluyl-CCl_2^+ (m/z 173, 175, 177).
[g]No signal observed for 10 and 1000 ug/mL; other significant ions observed are CCl_3^+ (m/z 117, 119, 121, 123) and RCl_2^+ (m/z 209, 211, 213).

where we assume that the ΔS term is insignificant since the DPT reaction (eq 3) is stoichiometrically neutral. Rearranging leads to the expression

$$\frac{[MH^+]}{[M^+]} = K\frac{[S]}{[S(-H)]} = e^{-\Delta H/kT}\frac{[S]}{[S(-H)]} \tag{7}$$

The ratio of $[MH^+]/[M^+]$ is dependent not only on K, but the ratio $[S]/[S(-H)]$. For CH_3OH solvent, ΔH ranges from about -0.5 to 1.0 eV for the five representative analyte molecules. As noted above K can be a very small number (energetically unfavorable). However, it is also easily seen that $[S]/[S(-H)]$ is very large since [S] is in high abundance and $[S(-H)]$ will be approximately equal to $[MH^+]$. By recognizing that the total yield of ions $[M^+] + [MH^+]$ is a function of the ionization efficiency ε of analyte concentration [M], the following equation is obtained;

$$\frac{[S(-H)]}{[S]} = f_m\varepsilon\frac{[MH^+]}{[M^+] + [MH^+]} \tag{8}$$

where f_m is the mole fraction of [M] relative to [S]. Solving for eq 8 leads to

$$\frac{[S(-H)]}{[S]} = \frac{K}{2}\left\{\left(1 + \frac{4f\varepsilon}{K}\right)^{1/2} - 1\right\} \tag{9}$$

Table 4 compares the calculated equilibrium ratios for the five test analyte compounds in MeOH expressed as MH^+ yield = $[MH^+]/([M^+] + [MH^+])$. The trends are in qualitative agreement with the measured results in Table 3. Naphthalene only weakly forms MH^+ whereas toluene and benzoic acid strongly form MH^+. [Toluene cation can undergo other chemistry that can complicate the interpretations above. It is also an excellent APPI dopant ion due to its propensity to deprotonate to a stable benzyl radical. Toluene cation can also convert to the 7-membered ring tropylium cation $C_7H_7^+$]. Aniline and phenol are intermediate cases and the equilibrium yield of MH^+ is strongly dependent on temperature and concentration. The column in Table 4 that most closely reflects the experimental conditions is that for a mole fraction of 10 ppm (about 30–40 μg/mL). At a vaporizer temperature of 200 °C, kT is about 0.04 eV giving values of K of 1.2×10^{-11} (naphthalene) to 1.3×10^{-6} (toluene); benzoic acid being the lone compound with a $K > 1$ value (8.3×10^4).

Finally we examine a few dependencies of the MH^+ yield. In Table 4 it is clear that MH^+ is favored for increasing temperatures and decreasing M concentration. In Figure 10 are plotted the calculated yields of MH^+ and S(−H) as a function of concentration for aniline and phenol. These calculations bear out the qualitative interpretation of reaction (eq 3) that as M increases in concentration, the second-order dependence of the reverse DHT reaction versus the psuedo

Table 4. Calculated MH^+ yield for the test analytes in MeOH as a function of analyte mole fraction and temperature

	Mole fraction (ppm) Temp (C) ΔH (eV) for MeOH	10 100	100 100	10 200	100 200
Naphthalene	1.02	0.00	0.00	0.11	0.03
Aniline	0.79	0.13	0.04	0.81	0.44
Phenol	0.62	0.83	0.46	1.00	0.96
Toluene	0.55	0.97	0.81	1.00	0.99
Benzoic acid	−0.46	1.00	1.00	1.00	1.00

first-order dependence of the forward DHT reaction with M would predict that relative MH^+ yield should decrease at higher M concentration. Although systematic concentration measurements were not performed on aniline or phenol, such measurements were made for 1-aminonaphthalene and phenanthrene in MeOH. These data plotted in Figure 11 indeed show the predicted trend in the relative MH^+ yield with concentration. However, the shape of the curve is not reproduced. In particular, the concentration dependence is only evident at higher concentrations; the relative MH^+ yield is approximately constant below 10 μg/mL. This may be due to kinetic limitations in that the very slow reverse reaction may mean that equilibrium takes longer with decreasing concentration. We consider this issue next.

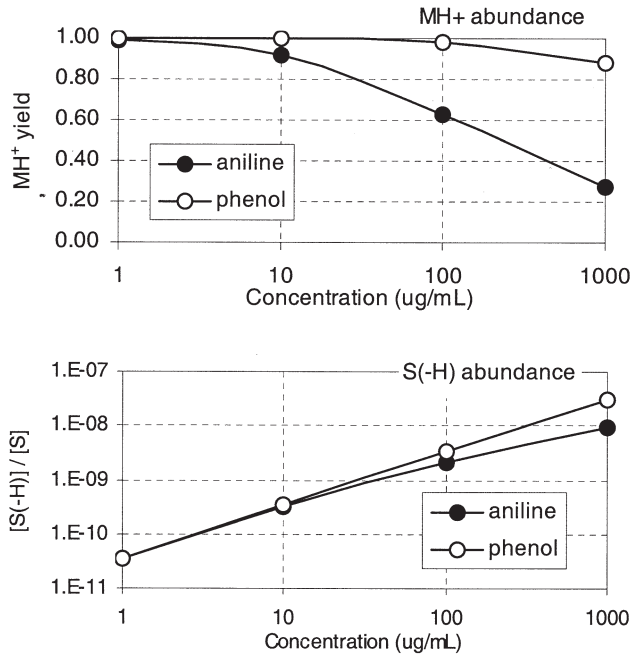

Figure 10. Calculated abundances of key species by the DHT mechanism for analyte molecules aniline and phenol as a function of analyte concentration in MeOH solvent. (Top) MH^+ yield. (Bottom) Relative yield [S(−H)]/[S]. Calculated abundances assume a photoionization efficiency of 10^{-4}, temperature of 200 °C, and ΔH values from Figure 9.

Kinetics Considerations

Interestingly, on purely energetic considerations, MH^+ formation appears very unlikely, whereas the equilibrium considerations above suggest that MH^+ production should be greater than is observed. The next physical process to consider is the kinetics of reaching equilibrium. We should expect slow kinetics due to the endothermicity of the DHT reaction. To model the rate of approach to equilibrium for reaction (eq 3), we evaluate the forward reaction rate, which leads to the equation

$$[MH^+]_t = [M^+]_0\left(1 - e^{-[S]k_f t}\right) \quad (10)$$

where [S] is the concentration of the hydrogen donating solvent and is assumed to be constant since [S] >> $[M^+]$, and k_f is the forward rate constant for DHT reaction (eq 3). The exponential lifetime of eq 10 is given by $1/t_e = k_f[S]$, which in turn can be expressed as

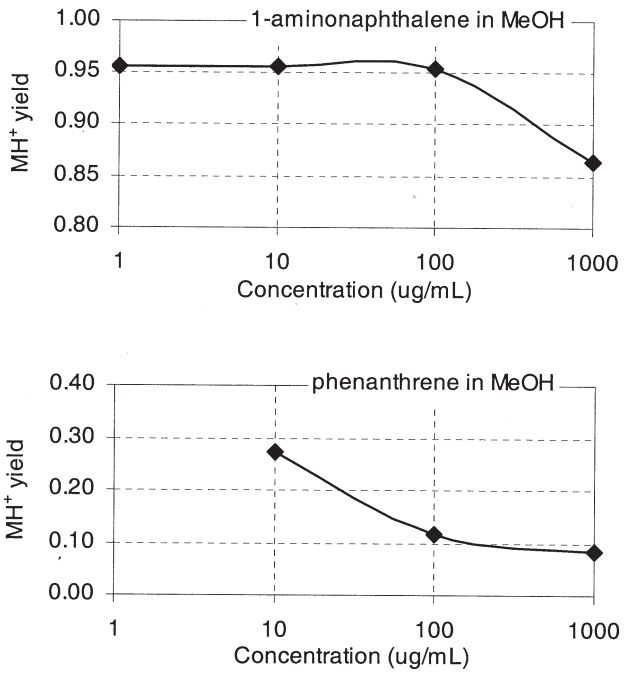

Figure 11. Measured MH^+ yield as a function of concentration for 1-aminonaphthalene and phenanthrene in MeOH.

$$k_f[S] = Ae^{-E_a/kT} \quad (11)$$

A is the pre-exponential factor, which for this bimolecular gas-phase reaction is the collision frequency of M^+ and S, and E_a is the activation energy, which for simplicity we assume is equal to ΔH.

We now estimate the timescale for reaching equilibrium. The LPPI source operates at about 2 torr, which gives a solvent concentration of [S] $\sim 7 \times 10^{16}$ molecules/cm^3. The kinetic energy imparted to the M^+ ion in the LPPI extraction field of 15 V/cm is about 0.06 eV based on a mean-free path of ~0.004 cm. The collision frequency A is dependent on the collision cross-sections σ of M^+ and S, which in turn are dependent on the hard-sphere diameters and the ion-molecule attractive potential. The hard-sphere cross section for an *m/z* 128 ion colliding with MeOH is approximately $\pi[(1 + (128/32)^{1/3})r]^2 = 5 \times 10^{-15}$ cm^2 where we assume r = 0.16 nm for MeOH. This leads to a value of $A = 1 \times 10^7$ collisions/s for a given ion M^+ at T = 400 K. This is a lower limit since the attractive potential greatly increases the effective collision cross section at these relatively low translational energies. Assuming a value of $E_a = \Delta H = 0.6$ eV (Table 4) and assuming that the effective kT in eq 11 from thermal (about 0.03–0.04 eV) and ion acceleration energy (about 0.06 eV) is 0.075 eV, we obtain a value of $t_e \sim 0.3$ ms. Given that the residence time of ions in the LPPI source is about 0.2 ms[16] and that t_e will be larger if $E_a > \Delta H$, it is possible that equilibrium is not fully achieved in the LPPI source used here.

Experimental evidence supporting the importance of the kinetic rate on the observed MH^+/M^+ ratio can be found in Figure 6, which shows that the hydrogen abstraction reaction requires a reactive length on the order of the LPPI dimensions. Otherwise the ions formed near the exit aperture would show more reaction. On a related note it is worth mentioning that the kinetics may be faster for APPI sources depending on the concentration [S], temperature and ion acceleration.

On the whole, the following statement summarizes the DHT mechanism for producing MH^+. The chemistry is energetically unfavorable, however, equilibrium prevails to make this a significant mechanism. The equilibrium of this reaction occurs slowly relative to the residence time of M^+ in the LPPI source thereby leading to a lower relative yield of MH^+ than predicted by the equilibrium model.

The Role of Ion-Molecule Complexes

The simple bimolecular gas-phase thermochemical and equilibrium model for DHT reaction (eq 3) understates the true complexity of the chemistry. Other chemical reactions may contribute to the results. It was evident that certain analyte ions and solvents lead to unanticipated products other than MH^+ (see footnotes to Table 3). However, in many cases, the ions are chemically well behaved leading primarily to M^+ and MH^+ only.

The overall agreement of the experimental results with the model for DHT reaction (eq 3) argues for the predominance of this mechanism in the formation of MH^+ by photoionization of M. However, other reactions can occur. The greatest discrepancies between the experimental results and the DHT model were for (1) the reversal in predicted MH^+ yield for aniline (higher than expected) versus phenol (lower than expected) and (2) much greater yield of MH^+ than predicted for the solvent H_2O. Some of this may be due to kinetic effects. Also these results are consistent with the results of Figure 8, which indicate that PA correlates more strongly with DHT than IE (for example, PA is 8.51 eV for phenol and 9.09 eV for aniline, Table 2).

Another mechanism that needs to be addressed is the process of ion-molecule complexation. The ion-molecule bond energy for hydrogen bonding molecules is on the order of 1 eV [18]. Subsequent solvent molecules may bind with decreasing bond energy (about 0.2-0.4 eV).[18] These are strong enough bond energies for significant ion-complex lifetimes to persist even at high temperatures. We examine the ion-complex DHT mechanism represented generally as

$$\begin{aligned} M^+ \cdot S_n &\rightarrow MH^+ \cdot S_{n-1} + S(-H) \\ &\rightarrow \rightarrow MH^+ + (n-1)S + S(-H) \end{aligned} \quad (12)$$

This reaction was studied by Syage for M = aniline and S = MeOH along with other solvents [19]. The thermochemistry was modeled using known stepwise solvation energies [20] and the experiment was conducted using ion-molecule complexes (clusters) generated in a supersonic expansion, ionized by resonance-enhanced multiphoton ionization (REMPI) or by electron ionization (EI) and then mass analyzed by TOFMS. Because REMPI excitation is through the first excited electronic state of aniline, the ionization process is clearly formation of M^+. It was observed that MeOH was an effective source of H atom to form MH^+ for aniline. The threshold complex size was $n = 3$ for REMPI excitation (relatively soft) and $n = 1$ for EI excitation (presumably due to the greater excitation energy). The M^+ ions are not accelerated during the reactive period in these ion complex studies whereas they are in the LPPI source. It is reasonable then that MH^+ would form for values of $n = 1$.

Steadman and Syage also studied the stepwise solvation reaction (eq 10) for the analyte M = phenol ionized by REMPI [21]. The DHT mechanism was not significant for phenol cation clusters as evidenced by the predominance of the M^+S_n series of ions (rather than MH^+S_{n-1} series) for solvents H_2O, CH_3OH, and NH_3. This work also revealed that deprotonation of phenol cation is an important reaction, much more so than for aniline, particularly in the presence of basic solvents. (Deprotonation of phenol cation by ammonia

molecules in cluster ion reactions was also reported by Mikami and coworkers [22]). Furthermore, solvent clustering about MH^+ can also deprotonate the ion due to the aggregate proton affinity of the solvent cluster. This may explain the observed low yield of MH^+ for phenol, since the PA is relatively low. These observations highlights that a more complete accounting of the potential reactions of M^+ with the surrounding vapor needs to be undertaken.

One conclusion of these observations is that ion-complexes can occur at high temperature and the chemistry that can ensue needs to be considered when developing a model for reaction (eq 3). Bruins and coworkers have obtained evidence that solvent complexation may assist in the charge transfer process that is key to the dopant model of analyte protonation [14]. One experiment to investigate this model would be to vary the electric fields in the LPPI source in order to impart variable kinetic energy, much greater than thermal energy, in order to disrupt the ion-complex reaction mechanisms.

Summary and Conclusion

This paper attempts to lay a foundation for understanding the complex chemical processes that occur in atmospheric pressure ionization (API) sources. The topic addressed here is the mechanism of MH^+ formation by direct photoionization. Experimental results were recorded using a low-pressure PI source that allowed us to more systematically examine ion-molecule chemistry relative to an APPI source. Based on these results and the thermochemical model developed here, we conclude that the mechanism is $M + h\nu \rightarrow M^+ + e^-$ followed by the reaction $M^+ + S \rightarrow MH^+ + S(-H)$. The principal experimental evidence for initial molecular radical ion formation M^+ followed by hydrogen atom abstraction from protic solvent S is:

1. Nearly exclusive formation of M^+ for headspace ionization of M in air
2. Significant relative abundance of MH^+ in the presence of protic solvents (e.g., CH_3OH, H_2O, c-hexane), but not in aprotic solvents (e.g., CCl_4)
3. Observation of pressure induced equilibrium oscillations in the abundance of MH^+ and M^+
4. Correlation of the ratio of MH^+/M^+ to reaction length in the photoionization source

Other evidence supporting the hydrogen abstraction mechanism of MH^+ includes the qualitative agreement between experimental and model predictions for the ratio of MH^+ yield to analyte concentration. However, the model is clearly elementary in its present form as evidenced by the results of Figure 8, which show that the MH^+ yield is more strongly correlated with proton affinity than the enthalpy of hydrogen abstraction. Furthermore it does not explain the efficiency of MH^+ formation in the presence of H_2O, which has a relatively high H-atom bond energy. These effects may reflect the importance of kinetics and the proton affinity may be strongly related to activation energy.

In summary, it is often difficult to know whether the absence of an expected ion is due to failure to ionize the molecule or due to subsequent ion-molecule chemistry, particularly for atmospheric pressure ionization sources. By deciphering these steps and understanding the thermochemical and kinetic properties of the ion-molecule reactions it may be possible to optimize the operation of not only APPI sources, but API sources in general.

Acknowledgments

The author thanks Karl Hanold (Syagen) and Andries Bruins (University of Groningen) for critical discussions. This work was partially supported by the National Science Foundation.

References

1. Syage, J. A.; Evans, M. D.; Hanold, K. A. Photoionization Mass Spectrometry. *Am. Lab.* **2000,** *32,* 24–29.
2. Robb D. B.; Covey, T. R.; Bruins, A. P. Atmospheric Pressure Photoionization: An Ionization Method for Liquid Chromatography-Mass Spectrometry. *Anal. Chem.* **2000,** *72,* 3653–3659.
3. Hanold, K. A.; Fischer, S. M.; Cormia, P. H.; Miller, C. E.; Syage, J. A. Atmospheric Pressure Photoionization (APPI). I. General Properties for LC/MS. *Anal. Chem.* **2003,** *76,* 2842–2851.
4. Syage,, J. A., Hanold,, K. A., Lynn,, T. C., Horner,, J. A., Thakur,, R. A. Atmospheric Pressure Photoionization (APPI). II. Dual Source Ionization. *J. Chromatogr. A,* in press.
5. Syage, J. A.; Hanning-Lee, M. A.; Hanold, K. A. A Man-Portable, Photoionization, Time-of-Flight Mass Spectrometer. *Field Anal. Chem. Tech.* **2000,** *4,* 204–215.
6. Syage, J. A.; Evans, M. A. Photoionization Mass Spectrometry—A Powerful New Tool for Drug Discovery. *Spectroscopy* **2001,** *16,* 14–21.
7. Syage, J. A.; Nies, B. J.; Evans, M. D.; Hanold, K. A. Field-Portable, High-Speed GC/TOFMS. *J. Am. Soc. Mass Spectrom.* **2001,** *12,* 648–655.
8. Raffaelli, A.; Saba, A. Atmospheric Pressure Photoionization Mass Spectrometry. *Mass Spectrom. Rev.* **2003,** *22,* 318–331.
9. Hayen, H.; Karst, U. Strategies for the Liquid Chromatographic-Mass Spectrometric Analysis of Non-Polar Compounds. *J. Chromatog. A 1000,* **2003,** 549–565.
10. Kauppila, T. J.; Kuuranne, T.; Meurer, E. C.; Eberlin, M. N.; Katiaho, T.; Kostiainen, R. Atmospheric Pressure Photoionization Mass Spectrometry. Ionization Mechanism and the Effect of Solvent on the Ionization of Naphthalenes. *Anal. Chem.* **2002,** *74,* 5470–5479.
11. Rauha, J-P.; Vuorela, H.; Kostiainen, R. Effect of Eluent on the Ionization Efficiency of Flavonoids by Ion Spray, Atmospheric Pressure Chemical Ionization, and Atmospheric Pressure Photoionization Mass Spectrometry. *J. Mass Spectrom.* **2001,** *36,* 1269–1280.
12. Kauppila, T. J.; Kotiaho, T.; Kostianen, R.; Bruins, A. P. Negative Ion-Atmospheric Pressure Photoionization-Mass Spectrometry. *J. Am. Soc. Mass Spectrom.* **2004,** *15,* 203–211.
13. Berkowitz, J. *Photoabsorption, Photoionization, and Photoelectron Spectroscopy;* Academic Press: New York, 1979.
14. Koster, G.; Bruins, A. P. Mechanisms for Ion Formation in LC/MS by Atmospheric Pressure Photo-Ionization (APPI). *Proceedings of the 49th ASMS Conference on Mass Spectrometry and Allied Topics;* Chicago, IL, May, 2001.

15. Marottaa, E.; Seraglia, R.; Fabris, F.; Traldi, P. Atmospheric Pressure Photoionization Mechanisms. 1. The Case of Acetonitrile. *Int. J. Mass Spectrom.* **2003,** *228,* 841–849.
16. Eiceman, G. A.; Karpas, Z. *Ion Mobility Spectrometry;* CRC Press: Ann Arbor, MI, 1994.
17. (a) Lias, S. G., Liebman, J. F., Levin, R. D. *J. Phys. Chem. Ref. Data* **1984,** *13,* 695. (b) Lias, S. G.; Bartmess, J. E.; Liebman, J. F.; Homes, J. L; Levin, R. D.; Mallard, W. G. *J. Phys. Chem. Ref. Data* **1988,** *17,* 1. (c) McMillen, D. F.; Golden, D. M. *Ann. Rev. Phys. Chem.* **1982,** *33,* 493. (d) *NIST Chemistry WebBook;* NIST Standard Reference Database Number 69, March 2003 Release.
18. Gonohe, N.; Abe, H.; Mikami, N.; Ito, M. Two-Color Photoionization of van der Waals Complexes of Fluorobenzene and Hydrogen-Bonded Complexes of Phenol in Supersonic Jets. *J. Phys. Chem.* **1985,** *89,* 3642.
19. Syage, J. A. Stepwise Solvation of Reactive Aniline Cation. *J. Phys. Chem.* **1989,** *93,* 170–79.
20. (a) Kebarle, P. *Ann. Rev. Phys. Chem.* **1977,** *28,* 445. (b) Grimsrud, E. P.; Chowdhury, S.; Kebarle, P. *Int. J. Mass Spectrom. Ion Processes* **1986,** *68,* 57–70.
21. Steadman, J.; Syage, J. A. Picosecond Studies of Proton Transfer in Clusters. 2. Dynamics and Energetics of Solvated Phenol Cation. *J. Am. Chem. Soc.* **1991,** *113,* 6786–95.
22. Mikami, N.; Okabe, A.; Suzuki, I. Photodissociation of the Hydrogen-Bonded Heterodimer Ion $[C_6H_5OH - NH_3]^+$. *J. Phys. Chem.* **1988,** *92,* 1858.